Porous structures in aspects of transpirating cooling of oxycombustion chamber walls

Cite as: AIP Conference Proceedings **2077**, 020065 (2019); https://doi.org/10.1063/1.5091926
Published Online: 21 February 2019

Paweł Ziółkowski

Porous Structures in Aspects of Transpirating Cooling of Oxycombustion Chamber Walls

Paweł Ziółkowski [1,2 a)]

[1]*Department of Energy and Industrial Apparatus, Faculty of Mechanical Engineering, Gdansk University of Technology, Narutowicza 11/12, 80-233, Gdansk, Poland*
[2]*Energy Conversion Department, Institute of Fluid Flow Machinery PAS-ci, Fiszera 14 St. 80-231 Gdańsk, Poland*

[a)]Corresponding author: pawel.ziolkowski@imp.gda.pl

Abstract. A wet oxycombustion chamber, which must be effectively cooled due to high temperature evolved during the oxy-combustion process, by using the phenomena of Reynolds thermal transpiration and Navier slip velocity. Closures needed to execute mass flow rate in a microchannel, which should be treated as a single porous structure in the walls of the combustion chamber, have been obtained by applying a local 3D approach. The Navier-Stokes model of the surface layer, which has been proposed and implemented, and presented in numerous publications has been used. The most important part was the incorporation of the thermal mobility force into the commercial code. The Computational Fluid Dynamic simulation of the benchmark experiment has been performed for basic data corresponding to helium. An original and easy-to-implement method has been developed to numerically confirm that at the final equilibrium zero-flow state there is connection between the Poiseuille flow in the centre of channel and the counter thermal transpiration flow at the surface. Therefore, the numerical implementation of the Reynolds model of thermal transpiration and its usefulness for the description of the benchmark experiment has been established. Additionally, taking Reynolds', Navier's and Poiseuille's solution into consideration for round capillary pipe flow, the flow enhancement due to the temperature difference at the surface and the presence of a drop (slip), can be easily identified. Nevertheless, these issues demand further work and calibration through dedicated experiment.

INTRODUCTION

The development of highly efficient and compact power generation systems requires the design of equipment that uses the effects of increased energy conversion. A good example of a concept taking the above into account is the double Brayton cycle with oxy combustion and carbon capture. The core and new elements of this innovative solution are the wet combustion chamber and the spray-ejector condenser. In order to carry out a wet combustion chamber balance, one has to come out of 3D equations with particular emphasis on surface phenomena, which play a leading role here. We can talk about enhanced energy conversion when the size of the device is reduced, in which the same transformation takes place quantitatively, but qualitatively it is a much intensified process. In the works [1-3] the model of increased transport on the nano-scale was presented, in which boundary conditions were determined, the expression in the form of friction and fluid stresses was formulated and the effect of transpiration was discussed. A model of temperature jump, a model of component concentration jump and an electric current jump model were presented. Motivations and examples of works indicating that this is the right direction of research are presented in the next section.

For a long time man dreamt of such a subjugation of nature, that he could safely control it and manage it in a convincing manner [4]. In order to do this, he needs devices of extraordinary power, with many times greater flow capacity, huge volume, with instant transformation of chemical, optical and thermal. In all these unusual devices, energy conversion is carried out, different from that known in classical pumps, turbines, compressors, reactors and boilers. Their common feature is the enormous density of energy, both that stored inside the working substance and that exchanged during the transformations. Therefore, today we are talking about " enhanced energy conversion",

Scientific Session on Applied Mechanics X
AIP Conf. Proc. 2077, 020065-1–020065-9; https://doi.org/10.1063/1.5091926
Published by AIP Publishing. 978-0-7354-1805-9/$30.00

hence the problem of understanding and mathematical modelling of the essence and nature of its increased transformation [5].

Below are the works of selected authors of basic character, focused on the problem of energy conversion understood more broadly than before. Such a vast plane of understanding, through the theoretical tools of enhanced post-Newtonian mechanics, allows to understand the mechanisms of phenomena leading to enhanced conversion. The current global research [6-11] shows the inevitability and necessity of creating a new branch of knowledge, which should be called: quantum thermodynamics, comprehensively capturing the phenomena occurring at the nanoscale.

The starting point for research into the phenomena in porous structures can be fuel cells, in which the chemical energy of fuel is directly converted into electricity, with an efficiency of up to 60-70% (hybrid systems in combination with a gas turbine). In order to be able to improve and correct them, however, it is necessary to understand and discover the principles on which they operate, namely the area of connection of anode, electrolyte and cathode. Generally speaking, intensification may be triggered by effects of slippage, mobility, transpiration, jumps and other little experimentally recognized effects in catalytic flows, new to theoretical modelling.

The model developed in this paper is based on new state equations - with more complex than the classic equations of the state of working mediums - for example, thermodynamic pressure is no longer a spherical tenor, and has components depending on the metric, curvature and bi- curvature of the contact surface. Much more thermodynamic reasonable definitions of osmotic pressures, wetting angles, three-phase lines of intersections, surface streams of pseudo-power and pseudo-energy, etc [1,2] arise here. The result is a thermodynamic excused object, responsible only for reversible phenomena - the surface stream of momentum. This stream, together with the newly defined surface stream of mass, entropy and `energy, is the surface analogy of Euler's fluid equations [1,3].

Modeling of irreversible phenomena of the Navier-Stokes layer is even more demanding - we are dealing with induced anisotropy forcing the presence of new coefficients unknown for isotropy [1-3]. Surface forces are anisotropic in nature. Therefore, it is worthwhile to introduce three frictional forces, which are independent in their essence: Duhema, Naviera and du Buata. Their dimensionless characteristics can be called Duhem, Navera and du Buata [1-3]. This division of friction forces into three contributions gives an opportunity to explain the phenomena observed by von Rybczyński and von Piotrowski over a hundred years ago [4]. The most important equations and basics of transition from 3D models on the surface to 0D models of the whole cycle are presented in the next section.

The phenomena of transpiration - including Reynolds thermal transpiration, Grahan's pressure and component transpiration, electrical transpiration and phase transition transpiration - should also be considered separately [1,3].

Table 1. shows:

1) names of transpiration phenomena;
2) description of mobility forces appearing on the boundary of two continuous bodies and
3) the potentials that drive these processes.

TABLE 1. Fife kinds of motions connected with a surface mobility of a particle immersed in a rest fluid. Here: $c_{m\theta}$ - the thermo-mobility coefficient, c_{mY} - the concentration-mobility coefficient, $c_{m\phi}$ - electro-mobility coefficient, $c_{m\varpi}$ - the pressure-mobility coefficient, c_{mx} - the phase mobility coefficient.

Phenomena	mobility forces	deriving potential
pressurephoresis	$\mathbf{f}_{m\varpi} = c_{m\varpi}\,\mathrm{grad}_s\,\varpi$	pressure ϖ
diffusionphoresis	$\mathbf{f}_{mY} = c_{mN}\,\mathrm{grad}_s\,Y$	concentration Y
thermophoresis	$\mathbf{f}_{m\theta} = c_{m\theta}\,\mathrm{grad}_s\,\theta$	temperature θ
electrophoresis	$\mathbf{f}_{m\phi} = c_{m\phi}\,\mathrm{grad}_s\,\phi$	electric potential ϕ
phasephoresis	$\mathbf{f}_{mx} = c_{mx}\,\mathrm{grad}_s\,x$	order parameter x

It should be mentioned that two phenomena related to mobility were discovered by Graham, namely pressurephoresis in 1846 [12] and diffusionphoresis in 1849 [13]. An important detail concerning the pressurephoresis is the fact that the focal pressure ϖ is taken into account first of all. Another type of wall motion induced by $\mathrm{grad}_s\,\theta$ on the wall is Reynolds' thermal transpiration, who was the first to attempt to unify the description of all forms of transpiration [14]. In turn, the electrical potential of ϕ and its impact on the forces of mobility was considered in the works [15]. Phasephoresis, on the other hand, is related to the change in the parameter of the state of matter which was presented in gradient models [16]. All these types of mobility are caused by the surface interactions of two

adjacent bodies and are generally referred to in the literature as the phenomena of phoresis motion [17]. One can also find potentials in the form of fields which, acting on a dipole, induce a moment ensuring magnetophoresis [18] or dielectrophoresis [19] (Table 6.2.).

TABLE 2. Two kinds of angular motions connected with a surface mobility of a particle immersed in a rest fluid. Here: $k_{m\mathbf{B}}$ - the magneto-mobility coefficient, $k_{m\mathbf{E}}$ - the dielectro-mobility coefficient.

Phenomena	mobility forces	deriving potential
magnetophoresis	$\mathbf{q}_{m\mathbf{B}} = k_{m\mathbf{B}} \operatorname{grad}_s \mathbf{B}$	magnetic field $\mathbf{B}$
dielectrophoresis	$\mathbf{q}_{m\mathbf{E}} = k_{m\mathbf{E}} \operatorname{grad}_s \mathbf{E}$	electric field $\mathbf{E}$

MATHEMATICAL MODELING

Regardless of the local, three-dimensional modeling, work should be carried out to address the issues of increased conversion in an integral way - at the level of the whole device or the whole turbine set, or thermodynamic cycle. It turns out that new energy, entropic or exergetic evaluations of these innovative solutions are needed. Thermodynamics, regardless of the way we practice it, receives powerful impulses for the development and elaboration of new research tools. Therefore, the next section presents the most important information on how the transition from 3D to 0D has been made in order to make a proper energy assessment of the issues of enhanced energy conversion. Dependences between modern dedicated computational tools as both for scientific researchers and for industrial applications are presented in Fig. 1. Developed four different branches of computational science which we nowadays call: CFD (Computational Fluid Dynamics); CSD (Computational Solid Dynamics); CFM (Computational Flow Mechanics); CSM (Computational Structure Mechanics) is still in progress [20].

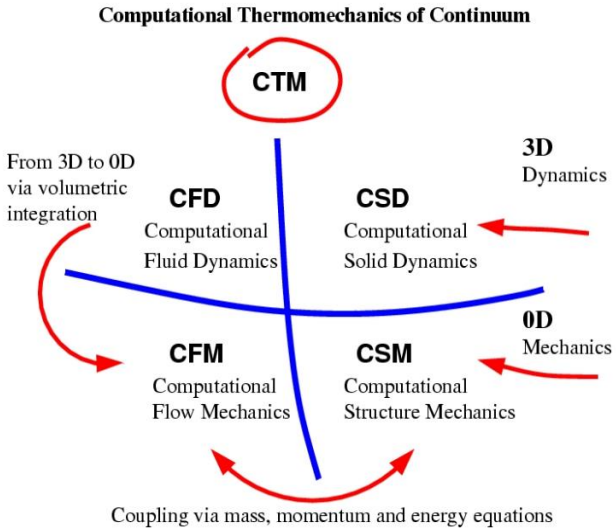

FIGURE 1. Internal relationship between four branches.

The coupling between a solid and a fluid takes place through interaction balances of mass, momentum and energy in the contact layer, which was presented in papers [20-22]. The literature uses the name FSI (Fluid-Solid Interaction) in the context of the general fluid-solid interaction. Especially important is the transmission of information on the interphase surface (working medium - construction), which is a connection and at the same time a boundary condition between CSD and CFD. Strength analyses of CSD derive data from CFDs and can simultaneously influence the character of the flow due to displacements. CFD analyses, on the other hand, affect a solid body, changing the stress state in it, which is shown in Fig. 1.

The transition from 3D to 0D was partially described in [23]. At this point it is worth mentioning that the phenomenon accompanying calculations based on 3D models is the renaissance of meaning and almost complete return to the equivalent significance of calculation codes based on 0D models. It should be remembered that the 0D codes covering the whole turbine and the block, thus serve the 3D codes (for both fluid and solids) as a " giver" of boundary conditions and averaged (in the sense of 0D) load data. What is more, also the results of 3D calculations, after appropriate averages, are compared with the results of 0D codes, especially at the stage of designing the solution, when we do not have any measurement data yet [24]. Example of results in 0D code was presented in Figure 2.

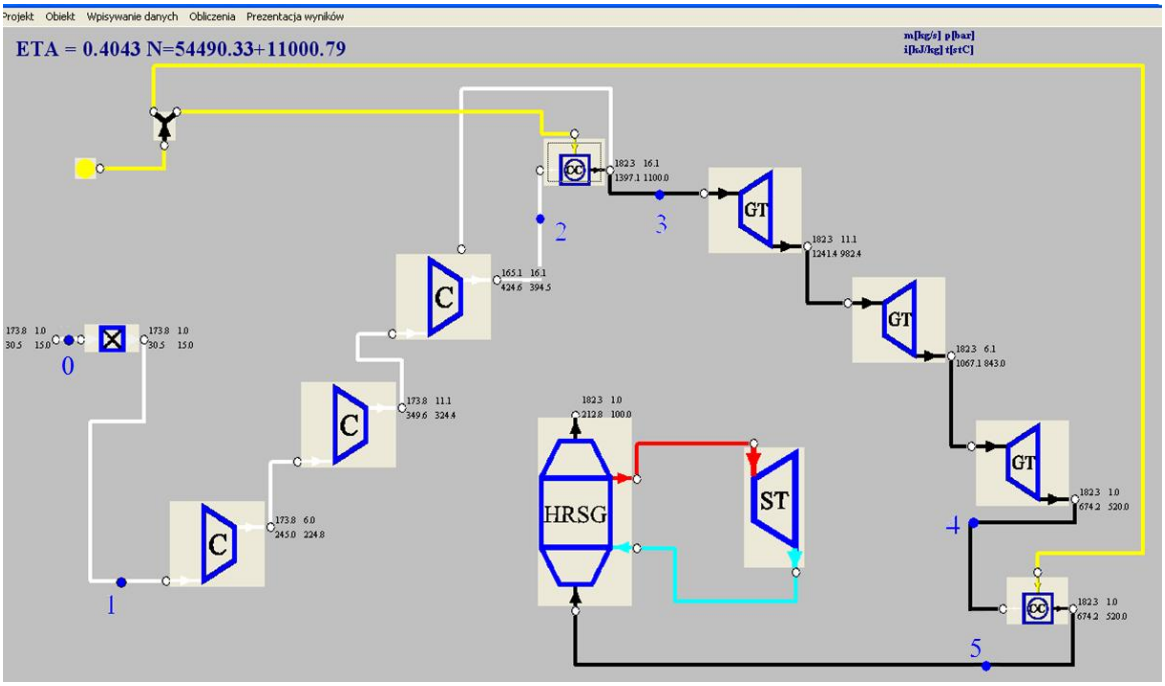

FIGURE 2. Scheme of gas-steam combined cycle calculated in 0D approach, where: C – compressor; CC – combustion chamber; GT – gas turbine; ST – steam turbine; HRSG – heat recovery steam generator.

There has been presented combined gas-steam cycle, however for a zero-emission power plant with oxy-combustion and carbon capture, are needed additional devices. The most important new devices is wet combustion chamber presented in Figure 3. The typical inert gas is replaced by water, which is introduced into the combustion chamber through its' porous structure, in conjunction with a cooling mixture composed of combusted fuel, that is steam with CO_2, and oxygen. It should be added that the zero-emission power plant with oxy-combustion and carbon capture, which can be called double Brayton cycle (DBC), consists of a traditional Brayton cycle (BC) and a second inverted Brayton cycle (IBC). The term 'inverted cycle' refers to a change in the order of the compressor and the turbine. Expansion of the medium occurs in the expander (GT^{in}) and then regeneration occurs in the heat exchanger (HE^{in}), heat rejection then occurs in the condenser (CON^{in}), and finally, compression of carbon dioxide occurs in the compressor (C^{in}). The main disadvantage of the whole system is the necessity for an air-separation unit (ASU), to supply the combustion chamber with pure oxygen.

In the first step, the optimal low pressure of double Brayton cycle, with oxycombustion and water injection in the combustion chamber and with a conventional condenser, has been determined to maximize the power output of the steam-gas turbine. The pressure and mass flow rates (fuel, oxygen and water) of the heat source in the combustion chamber have been given and presented in preceding works [25,26]. Therefore, the concept of the development of Computational Flow Mechanics (CFM) codes has been moving towards inclusion closures obtained at a more sophisticated level using local 3-dimensional approaches. Main reason for introducing these closures is connected

with a lack of knowledge about proper modelling at design level of such phenomena as Reynolds thermal transpiration in porous structures.

Wet Oxycombustion Chamber

Analysis of the proposed double Brayton cycle has been shown to predict the influence of the phenomena which occurs in two new devices, specifically (1) a wet combustion chamber using oxy- combustion and water cooling by thermal transpiration (in the porous walls of the combustion chamber there is no relevance associated with typical bulk phenomena, since the whole flow is dominated by surface processes, for example, Navier slip and Reynolds transpiration) and (2) a spray-ejector condenser (condensation of steam from gas-steam medium occurs due to the contact with surface injected water). Therefore enhanced energy conversion is possible in the two devices with high volumetric surface density which is novel in comparison to typical gas turbines cycles.

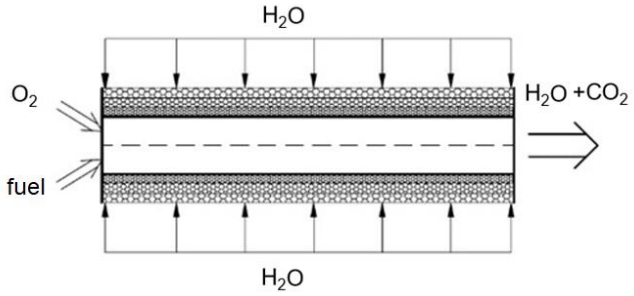

FIGURE 3. The wet combustion chamber using oxy- combustion and water cooling by thermal transpiration (in the porous walls of the combustion chamber there is no relevance associated with typical bulk phenomena, since the whole flow is dominated by surface processes).

The double Brayton cycle efficiency is defined as a quotient of the electrical power generated by the double Brayton cycle and the fuel chemical energy flux contained in the fuel and is obtained by η_{el-DBC}= 52.3%. However, the entire system efficiency falls by around 8.66% due to the production of oxygen (6.38%) and the capture of CO_2 (2.28%). Therefore, the analysis of the gas-steam turbine with oxy-combustion, water injection and inverted Brayton cycle shows that the optimal efficiency value $\eta_{el-netto}$= 43.67% for the entire block was identified as occurring at a pressure of p = 7.8 kPa in the condenser. The main advantage of this solution is the lack of emissions such as carbon dioxide and nitrogen oxides. The obtained efficiency of a zero-emission cycle with the spray-ejector condenser amounts to about η_{el-SEC}=37.78%. The drop in efficiency is equal to 5.91 percent in comparison to a cycle with a conventional steam condenser, however the proposed innovation of the discussed cycle provides an increase of approximately 32 times the volumetric heat flux density. Hence, the results of the thermodynamic analysis indicates the legitimacy of building cycles based on enhanced energy conversion [25,26].

Governing Equations

The concept of closures needed to execute mass flow rate in a microchannel, which should be treated as a single porous structure in the walls of the combustion chamber, have been presented in Fig. 4. As was mentioned before, project of enhanced energy conversion involves a wet combustion chamber, which must be effectively cooled due to high temperature evolved during the oxy-combustion process, by using the phenomena of Reynolds thermal transpiration and Navier slip velocity. This part of the analysis is based on the Navier-Stokes model of the surface layer, which has been proposed and implemented within the preceding publications [1-3].

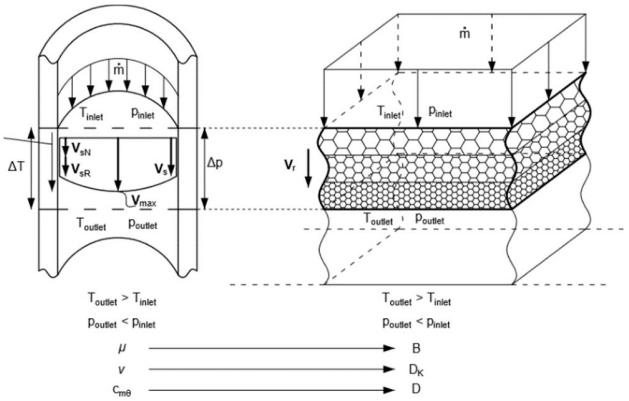

FIGURE 4. Concept of using resolution from single microtube into porous structure in the walls of the oxycombustion chamber.

However, the most important part of this reasoning should be presented. Treating that a laboratory nano or micro-pipe is fully equivalent to a single porous channel and looking for common effects of the bulk and surface motion, one may consider of a following momentum flux integral in any cross section of a porous media oriented by tangential component of unit vector $\mathbf{n}_{\tan}$:

$$\iint\limits_{\text{bulk section}} (\rho \mathbf{v}\otimes\mathbf{v} + \mathbf{p})\mathbf{n}_{\tan} dA + \oint\limits_{\mathcal{L}} (\rho_s \mathbf{v}_s \otimes \mathbf{v}_s + \mathbf{p}_s + \mathbf{p}\,\mathbf{n}_{\text{nor}} + \mathbf{f}_{\partial V})\mathbf{n}_{\tan} d\mathcal{L} = 0 \tag{1}$$

In the above $\rho\mathbf{v}$ and $\rho_s\mathbf{v}_s$ are the bulk and the surface momentum density vectors, ρ and ρ_s are the gas density in the bulk and on the boundary. Next, $\mathbf{p} = p_{ij}\,\mathbf{e}_i \otimes \mathbf{e}_j = \mathbf{p}^{\mathrm{T}}$ and $\mathbf{p}_s = \mathbf{p}_s{}^{\mathrm{T}}$ are the bulk and the surface flux of momentum. The boundary force can be separated on: surface friction and surface mobility, thus: $\mathbf{f}_{\partial V} = \mathbf{f}_r + \mathbf{f}_m$ [1-3]. A total momentum influx as to be :

$$\mathcal{M} = \iint\limits_{\text{bulk section}} \rho \mathbf{v} v_{\tan} dA + \oint\limits_{\mathcal{L}} \rho_s \mathbf{v}_s v_{s\,\tan} d\mathcal{L} \tag{2}$$

$$\mathcal{M} = \dot{m}\boldsymbol{v}_r \tag{3}$$

Where $\iint_{\text{bulk section}} \rho \mathbf{v} v_{\tan} dA$ - contribution from bulk velocity and $\oint_{\mathcal{L}} \rho_s \mathbf{v}_s v_{s\,\tan} d\mathcal{L}$ - contribution from the slip velocity $v_{s\,\tan} = \mathbf{v}_s\,\mathbf{n}_{\tan}$. Using some arguments from technique of homogenization, we can postulate an existence of a resultant velocity $\mathbf{v}_r$, which is parallel to the vector of total momentum (3). This vector is located somewhere in a geometrical center of a velocity profile. In many cases, independently of the shape of the cross section the bulk profile of velocity is nearly flat and ending with value of $v_{s\,\tan} \approx |\mathbf{v}_s|$ - the magnitude of slip velocity. In the above, according with traditional Reynolds notation, $\dot{m}$ denotes resultant mass flow rate. Taking into account that $\mathbf{f}_{\partial V} = \mathbf{f}_r + \mathbf{f}_m = \nu(\mathbf{v} - \mathbf{v}_{\text{wall}}) - (c_{m\theta}\,\text{grad}_s\theta_s)$ there can be reorganized the integral (2.1), expressing explicitly the thermal mobility part $c_{m\theta}\,\text{grad}_s\theta_s$ with the thermo-mobility coefficient $c_{m\theta}$ and the slip friction part $\nu\mathbf{v}_s$, where ν is the Navier surface friction coefficient :

$$\dot{m}\mathbf{v}_r = \iint\limits_{\text{Poiseuille}} (p\mathbf{I} + \mu\mathbf{d})\mathbf{n}\, dA + \oint\limits_{\text{Darcy}} \nu\mathbf{v}_s\mathbf{I}_s\, d\mathcal{L} + \oint\limits_{\text{Reynolds}} c_{m\theta}\,\text{grad}_s\theta_s\, d\mathcal{L} \tag{4}$$

Since the porosity in any cross section of porous media is quite arbitrary, then the known procedure of homogenization can be applied, thus eq.(4) leads finally, to 3D resultant equation [3]:

$$\mathbf{v}_r = -\left(\frac{P}{\mu}\mathbf{B} + \mathbf{D}_K\right)\frac{\text{grad}\,P}{P} + \mathbf{D}\frac{\text{grad}\,T}{T} \tag{5}$$

where $\mathbf{v}_r$ is the resultant filtration velocity, μ is a gas viscosity, $\mathbf{B}$ is the permeability tensor, $\mathbf{D}_K$ is the Knudsen accommodation diffusion tensor and $\mathbf{D}$ is the thermal transpiration coefficient tensor. Additionally, P is the capillarity pressure and T is the capillarity temperature. Analogical coefficients are presented in Figure 4.

NUMERICAL EXAMPLE

For example to incorporate the thermal mobility force into the commercial code the thermo-mobility coefficient should be calibrated (see TABLE 1). The new benchmark experiment [27], which has applied an original method for thermal transpiration, induced mass flow rate measurements, conducted via measuring *in situ* the pressure evolution in real time at both ends of the tube using two high-speed response pressure gauges. A long, circular cross-section, glass (borosilicate) microtube ($d = 490$ μm; $L = 3.053$ cm) is connected between two reservoirs: cold (no 1, environmental temperature) and hot (no 2, $\theta_2 = 80$ °C, heated by an internal heater) (Figure 5) with the volume of the two reservoirs $V_H/V_C = 0.81$ and for numerical simulations $V_C = 14.85$ cm^3 was selected. Before experiment begins, the pressure inside the both reservoirs is regulated by means of a vacuum system and stays between 13.3 and 1330 Pa for helium. After the opening of the isolation valve, the flow induced by thermal transpiration is simple – the pressures in both reservoirs are equal and flow from cold to hot areas is derived only by the wall mobility force ($\mathbf{f}_m = c_{m\theta}\mathrm{grad}_s\theta_s$) which depends on the $c_{m\theta}$ value between glass and helium and the wall temperature gradient. The volume of the reservoirs under consideration are finite, therefore gas molecules migrate from cold to hot reservoirs. As the results of this migration pressure in the cold areas decreases and at the hot areas increases (see: Figure 6).

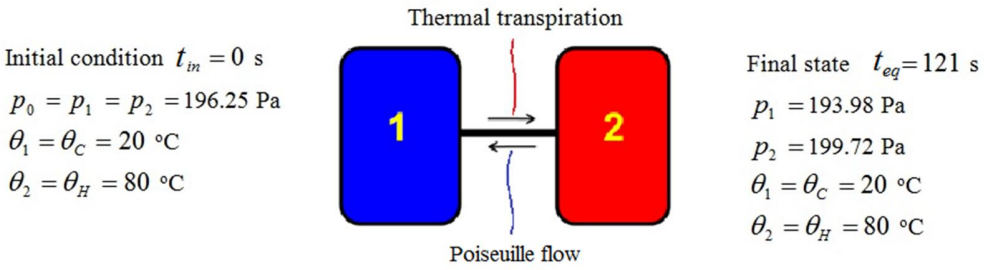

FIGURE 5. Scheme of helium flow cold (1) to hot (2) reservoir [27], where initial condition: environmental temperature (cold, no 1) and $\theta_2 = 80$ °C (hot, no 2) and pressure $p_1 = p_2 = p_0 = 196.25$ Pa for $t_0 = t_{in}$.

Considering the previous literature according to [28, 29], and keeping in mind the value of the thermal accommodation coefficient proposed in the literature [30, 31], there has been made a calibration of the $c_{m\theta}$ value. Drawing from the experimental data [27] and additional considerations [32], this coefficient has been found to have the following form:

$$c_{m\theta} = \frac{3}{4}\frac{\mu^2}{\theta\rho l_s} \tag{6}$$

Here the main unknown is the Navier slip viscosity ν that can also be defined by slip length l_s. It was assumed that the numerical value of $c_{m\theta}$ has been calculated using the definition of the Helmholtz-Piotrowski slip length: $l_s = \mu/\nu$, and helium-glass slip length $l_s = 0.00016$ cm. In equation (6) the temperature along the micro-pipe was taken according to linear distribution. For the implemented thermal transpiration and slip velocity condition at the wall, the numerical results agree very well with the experimental data for the pressure plots in Figure 6.

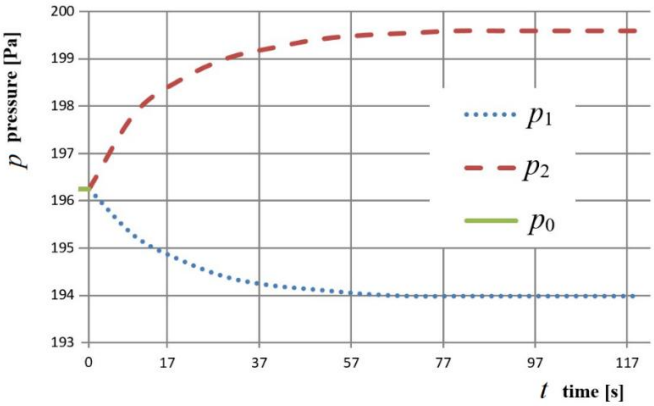

FIGURE 6. Plot of pressure change in the cold (1) and hot (2) reservoirs, where initial pressure p_0 = 196.25 Pa for t_0=t_{in}.

Also, during numerical simulations [30], it has been observed that the pressure variations inside both reservoirs are not perfectly mirror-symmetric with respect to the initial pressure axis, since the volumes of the two reservoirs differ (the hot is smaller). Consequentially, the pressure variation in time within the reservoirs is different – the increase in the hot (2) reservoir is to 199.72 Pa and decrease in the cold (1) reservoir is to 193.98 Pa (Figs. 5 and 6). An original and easy-to-implement method has been developed to numerically confirm that at the final equilibrium zero-flow state there is connection between the Poiseuille flow in the centre of channel and the counter thermal transpiration flow at the surface (see Figure 7).

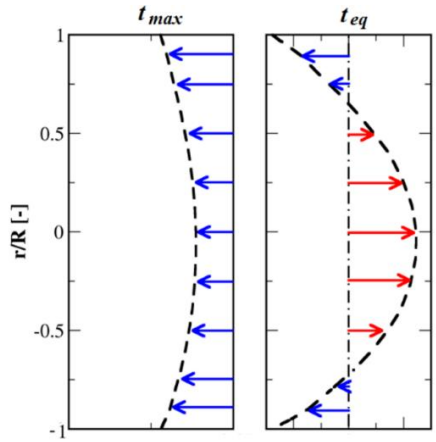

FIGURE 7. Plot of velocity profiles for two characteristic times, namely: t_{max} [s] time of maximum flow rate and t_{eq} [s] time of zero flow rate – equilibrium conditions $\dot{m} = 0$ [g/s]; where R = $d/2$ is a radius of microtube and r is a distance from the centre of microtube.

CONCLUSIONS

The CFD simulation of the benchmark experiment has been performed for basic data corresponding to helium. An original and easy-to-implement method has been developed to numerically confirm that at the final equilibrium zero-flow state there is connection between the Poiseuille flow in the centre of channel and the counter thermal transpiration flow at the surface. Therefore, the numerical implementation of the Reynolds model of thermal transpiration and its usefulness for the description of the benchmark experiment has been established. Additionally, taking Reynolds', Navier's and Poiseuille's solution into consideration for round capillary pipe flow, the flow enhancement due to the temperature difference at the surface and the presence of a drop (slip), can be easily identified. Nevertheless, these issues demand further work and calibration through dedicated experiment.

ACKNOWLEDGMENTS

The author would like to offer thanks to Prof. dr hab. inż. Janusz Badur of the IMP PAN in Gdańsk for his professional support and expert advice during the preparation of this article.

REFERENCES

1. J. Badur, M. Karcz, M. Lemański and L. Nastałek, CMES: Computer Modeling in Engineering & Sciences **73**, 299–310 (2011). doi:10.3970/cmes.2011.073.299.
2. J. Badur, M. Karcz and M. Lemański, Microfluidics and Nanofluidics **11**, 439–449 (2011).
3. P. Ziółkowski and J. Badur, Archives of Mechanics, **70**, 3, 269–300 (2018).
4. J. Badur, *Development of Energy Concept*, IMP PAN Publishers, Gdansk, 2009. (in Polish).
5. J. Badur, P. Ziółkowski, W. Zakrzewski, D. Sławiński, M. Banaszkiewicz, O. Kaczmarczyk, S. Kornet and P.J. Ziółkowski, On the surface vis impressa caused by a fluid-solid contact, [in]: Shell Structure Theory and Applications, red. W. Pietraszkiewicz & J. Górski **3**, 53-56, (2014).
6. J.R. Bielenberg and H. Brenner Journal of Fluid Mechanics, **546**, 1-23 (2006).
7. D.L. Morris, A. Hannon and A.L. Garcia Physical Review A, **46**, 5279-5282 (1992).
8. E.B. Arkilic, M.A. Schmidt and K.S. Breuer Journal of Microelectromechanical Systems **6**, 167–178, (1997).
9. G.L. Morini, M. Lorenzi, M. Spiga Microfluidics and Nanofluidics **1**, 190-196, (2005).
10. J. Pitakarnnop, S. Varoutis, D. Valougergis, S. Geoffroy, L. Baldas and S. Colin, Microfluidics and Nanofluidics **8**, 57-72, (2010).
11. G.E. Karniadakis, A. Beskok and N. Aluru, *Microflows and Nanoflows: Fundamentals and Simulation*, Springer, New York, 2005.
12. T. Graham, Philosophical Transactions of the Royal Society of London **131**, 573-632 (1846).
13. T. Graham, Philosophical Transactions of the Royal Society of London **137**, 349-362 (1849).
14. O. Reynolds, *On the equation of motion and the boundary conditions for viscous fluid* (1883), Scientific papers on mechanics and physical subjects Tome 2, 46, 132-137, Cambridge University Press, Cambridge, (1901).
15. M.V. Smoluchowski, Z. Phys, **17**, 557-585 (1916).
16. Z. Bilicki and J. Badur, Journal of Non-Equilibrium Thermodynamics, **28**, 145-172 (2003).
17. H. Brenner, Physica, **349**, 1/2, 60-132 (2005).
18. F. Yu, L. Zhang, Y. Huang, K. Sun, A. David and V.C. Yang, Biomaterials **31**, 5842-5848 (2010).
19. M. Lackowski and H. Nowakowska, Trans. IFFM No. **133**, 109–115 (2016).
20. J. Badur, P. Ziolkowski, D. Slawinski and S.Kornet, "An approach for estimation of water wall degradation within pulverized-coal boilers", Energy **92**, 142-152 (2015).
21. J. Badur, P. Ziolkowski, W. Zakrzewski, D. Slawinski, S. Kornet, T. Kowalczyk, J. Hernet, R. Piotrowski, J. Felicjancik and P.J. Ziolkowski, "An advanced Thermal-FSI approach to flow heating/ cooling", Journal of Physics: Conference Series **530**, 1-8 (2014). doi:10.1088/1742-6596/530/1/012039.
22. M. Banaszkiewicz, "Multilevel approach to lifetime assessment of steam turbines", International Journal of Fatigue **73**, 39–47 (2015).
23. J. Badur, *Five lecture of contemporary fluid termomechanics*, Gdańsk 2005. (in Polish)
24. J. Badur, *Numerical modeling of sustainable combustion in gas turbine*,(IMP PAN Publishers, Gdańsk, 2003).
25. P. Ziółkowski, W. Zakrzewski, O. Kaczmarczyk, J. Badur, Archives of thermodynamics, **34**, 2, 23-38 (2013).
26. P. Ziółkowski, "Thermodynamic analysis of low –emission gas-steam cycles with the use of oxy-combustion" Ph.D. thesis, Institute Fluid Flow Machinery PAS-ci, 2018.
27. M. Rojas-Cárdenas, I. Graur, P. Perrier and J.G. Meolans, Physics of Fluids, **25**, 031702, (2011).
28. P. Ziółkowski, J. Badur, Journal of Physics: Conference Series, **530**, 012035 (2014). doi:10.1088/1742-6596/530/1/012035.
29. J. Badur, P.J. Ziółkowski and P. Ziółkowski, Microfluidics and Nanofluidics, **19**, 191–198 (2015).
30. P. Ziółkowski and J. Badur, International Journal of Numerical Methods for Heat and Fluid Flow, 28, 1, 64-80, (2018). https://doi.org/10.1108/HFF-10-2016-0412.
31. J.M. Reese, Y. Zheng and D.A. Lockerby, Journal of Computational and Theoretical Nanoscience, **4**, 807-813, (2007).
32. T. Ewart, P. Perrier, P., I. Graur and J.G. Meolans, Microfluidics and Nanofluidics, **3**, 689-695 (2007).